JOURNAL OF THERMOPHYSICS AND HEAT TRANSFER
Vol. 16, No. 2, April–June 2002

Thermodynamic Model of Hydrazine that Accounts for Liquid–Vapor Phase Change

D. Giordano*
European Space Research and Technology Center, 2200 AG Noordwijk, The Netherlands
and
M. De Serio†
University of Bari, 70126 Bari, Italy

The work carried out to develop a thermodynamic model of hydrazine with the theoretically built-in capability to account for liquid–vapor phase transitions and suited for implementation in two-phase flow solvers is described. After introductory considerations of fluid dynamics aspects and thermodynamic stability, the method of constructing the model based on an assumed state equation $p = p(T, v)$ and of perfect-gas, constant-pressure, specific-heat data available from tables of thermodynamic properties published in the literature is described. The corresponding fundamental relation is given in terms of the Helmholtz potential. Subsequently, the liquid–vapor phase equilibrium is considered and resolved via equations in line with the standard thermodynamic principles of energy minimization or entropy maximization. Aspects of model validation are discussed with respect to the liquid–vapor saturation curve, vaporization enthalpy, density, and constant-pressure specific heat of the liquid phase. A description of other theoretical models published in the literature, together with a comparative analysis of their features relevant to the context of this work, is also included.

Nomenclature

A, B, C, n	=	state equation constants
a_k	=	interpolation coefficients, Eq. (26)
a_N	=	isothermal speed of sound
c_p	=	constant-pressure specific heat
c_v	=	constant-volume specific heat
f	=	Helmholtz potential
h	=	enthalpy
K_T	=	isothermal compressibility coefficient
K_1, K_2	=	integration constants
M	=	N_2H_4 molar mass, 32.045282×10^{-3} kg · mol^{-1}
p	=	thermodynamic pressure
R	=	hydrazine gas constant, 259.46 J · kg^{-1} · K^{-1}
s	=	entropy
T	=	absolute temperature
u	=	internal energy
V	=	volume
v	=	specific volume (mass)
Z	=	compressibility ratio
μ	=	chemical potential
$\hat{\mu}$	=	temperature-only dependent part of μ
$\tilde{\mu}$	=	specific-volume dependent part of μ
μ^*	=	nondimensional function related to μ
π	=	reduced pressure
π_m, π_M	=	minimum and maximum reduced pressure
ρ	=	mass density
τ	=	reduced temperature
τ_t	=	tangent-isotherm reduced temperature
$\Phi(T)$	=	perfect-gas constant-volume specific heat
ϕ	=	reduced specific volume
φ	=	reduced shifted specific volume
φ_m, φ_M	=	left and right limits of unstable-state ranges
$\varphi_{\mathrm{np,l}}, \varphi_{\mathrm{np,r}}$	=	left and right limits of negative-pressure ranges
$\psi(T)$	=	generic function of temperature

Subscripts

c	=	critical
l	=	saturated liquid
v	=	saturated vapor
vap	=	vaporization

Received 6 June 2001; presented as Paper 2001-3016 at the 35th Thermophysics Conference, Anaheim, CA, 11–16 June 2001; revision received 21 September 2001; accepted for publication 21 September 2001.

*Research Engineer, Aerothermodynamics Section, P.O. Box 299. Member AIAA.
†Researcher, Department of Chemistry, Via Orabona 4.

I. Introduction

THE availability of the thermophysical and thermochemical properties of hydrazine (N_2H_4) is always considered an important requirement in many engineering sciences that presuppose the use of this compound. A rather exhaustive description of the various applications of N_2H_4 can be found in the authoritative monograph written by Schmidt[1] in 1984. Notwithstanding the multitude and variety of such applications, N_2H_4 is most often associated with propulsion engineering, a domain in which the compound finds extensive use as a propellant. In this regard, aspects of major interest are undoubtedly those relative to its performance as a fuel in relation to the design of thrusters for spacecraft attitude control or orbit adjustment. There are, however, other aspects, namely, those relative to N_2H_4 storage in tanks and flow in feeding and/or venting lines of propulsion subsystems that may acquire critical importance under particularly severe environmental conditions, such as those encountered in outer space, and that demand careful consideration in consequence of the potential risks associated with undesirable phase changes that liquid N_2H_4 may undergo, in so doing, impairing the correct functioning of the subsystems.

The contents of the present paper bear on the latter aspects. The thermodynamic study described constitutes part of an ampler research activity called for by the necessity to assess the feasibility to evacuate into outer space the residual liquid N_2H_4 from the tanks mounted on the vehicle equipment bay (VEB) that feed the attitude control system (SCA) of the European rocket launcher ARIANE 5. This necessity arose because specific missions of the launcher had planned, at the end of the launch segment, the reentry of the VEB into the Earth's atmosphere and its consequent destruction in the denser

layers due to intense aerodynamic heating. Within this scenario, the residual liquid N_2H_4 still present in the spherical tanks represents an explosion hazard that must be prevented to avoid the production of space debris, in accordance to recently established and internationally agreed practices[2] on the use of outer space. A viable preventing action would be to vent the tanks by discharging the residual N_2H_4 into space before the VEB reentry. This approach, however, calls attention to a series of problems connected with the potential phase changes that liquid N_2H_4 may undergo because of the temperature and pressure drop, from given tank conditions, while flowing through the venting lines and at the moment of ejection into vacuum. In particular, the questions to address are if and where a phase change occurs, how to avoid it or, at least, how to allow it without impairing the venting process. These concerns are particularly acute in relation to the possible solidification, either directly from liquid or following evaporation, of N_2H_4 because of the associated pipe-clogging risk and ejection of finite-size solid particles into space. The need to find qualitatively meaningful and quantitatively accurate answers imposes the necessity to study numerically the liquid N_2H_4 flowfield in critical portions of the SCA venting lines with the supporting complement of experimental investigations.[3] In this regard, a mandatory ingredient for successful analysis is the availability of a thermodynamic model of N_2H_4 with the theoretically builtin capability to account for phase changes. The main purpose of this paper is to describe the work performed to develop a preliminary model applicable to liquid–vapor phase transition.

II. Fluid Dynamics Aspects

The motion of a continuous medium thermodynamically characterized by two specific state parameters is governed by the standard differential equations that represent the conservation of mass, momentum, and total energy. Apart from the assignment of the phenomenological equations for the diffusive flux of internal energy and the dissipative part of the stress tensor, the flowfield equations must be complemented with the fundamental relation[4–6] of the thermodynamic model assumed to represent the physical behavior of the real medium to provide functional dependencies among the variables of thermodynamic nature appearing in them. In this regard, alternative, although equivalent, formulations are possible. In view of the necessity to deal with state equations that are cubic with respect to specific volume ($v = 1/\rho$), there is an objective convenience to work out the mathematical details within the formalism of the Helmholtz-potential formulation. This choice presupposes the use of temperature and specific volume as independent state parameters. When the Helmholtz potential $f = f(T, v)$ is known in explicit form, pressure and internal energy follow simply from

$$p = -\left(\frac{\partial f}{\partial v}\right)_T = p(T, v) \tag{1}$$

$$u = -T^2\left(\frac{\partial f/T}{\partial T}\right)_v = u(T, v) \tag{2}$$

A necessary prescript for successful prediction of the flowfield is the ability of the thermodynamic model to represent in a physically consistent and accurate manner the behavior of the medium in the (T, v) region of interest to the particular application being considered. Thus, if the medium undergoes phase changes, then a satisfactory candidate to its representation should be a theoretical model for which the conditions of thermodynamic stability[4–8]

$$\left(\frac{\partial^2 f}{\partial T^2}\right)_v = -\frac{c_v}{T} < 0 \tag{3}$$

$$\left(\frac{\partial^2 f}{\partial v^2}\right)_T = \frac{a_N^2}{v^2} > 0 \tag{4}$$

can be violated in some points or loci of the considered (T, v) domain. As an example relevant to condensation and evaporation, consider the isotherms of the perfect-liquid,[9] van der Waals, and perfect-gas models in the (p, v) plane. The first stability condition [Eq. (3)] is always satisfied for these three models because their constant-volume specific heat never becomes negative. The second stability condition [Eq. (4)] is linked to the slope

$$\left(\frac{\partial^2 f}{\partial v^2}\right)_T = \frac{a_N^2}{v^2} = -\left(\frac{\partial p}{\partial v}\right)_T \tag{5}$$

of the isotherms. The perfect-gas model never violates the condition in question because the slope of the associated isotherm $[(\partial p/\partial v)_T = -RT/v^2]$ always stays negative; accordingly, such a model is always thermodynamically stable and does not possess the builtin capability of predicting condensation. A similar conclusion can be drawn also for the perfect-liquid model: It cannot predict evaporation because $(\partial p/\partial v)_T = -\infty$ and the stability condition [Eq. (4)] is once again never infringed. Even the introduction of a finite and constant coefficient of isothermal compressibility $[K_T = -v(\partial v/\partial p)_T = \text{const} > 0]$ does not remove the limitation; it merely confers a curvature to the perfect-liquid isotherm similar to that of the liquid branch of the van der Waals isotherm without, however, introducing a minimum. In turn, the van der Waals isotherm features a region of instability between the minimum and the maximum, where the stability criterion [Eq. (4)] is not satisfied $[(\partial p/\partial v)_T \geq 0]$ and the isothermal speed of sound becomes imaginary. According to the thermodynamic stability theory,[4–8] this is the "hallmark of a phase transition," as Callen (see Ref. 6) characteristically expressed it. Thus, the van der Waals model has built into it the physical information necessary to predict condensation and/or evaporation. Such a conclusion is true for all theoretical models whose state equation $p = p(T, v)$ shows a trend similar to van der Waal's. Accordingly, the models qualify as acceptable candidates to consider at the moment of choosing the one that represents the real medium. Note that the preceding considerations do not drastically preclude the use of the perfect-liquid and -gas models to determine the characteristic parameters of the condensation/evaporation phase transition in approximate calculation methods. As a matter of fact, this approach constitutes widespread practice for temperatures sufficiently below the critical temperature. The motivation supporting the discussion relative to the described example is that, within a fluid-dynamics context, the possible clash between physical incoherence or limitations carried by inadequate models and phase-change events taking place in the flow may occur in a very unforeseeable manner. Realization that simplified models are being misused outside the domain where they yield an acceptable approximation is not within easy control when running a flow simulation. Thus, to avoid such an undesirable and unnecessary risk, it is recommendable to employ theoretical models that offer unconditional internal coherence with the physics of phase change as an essential, although not sufficient, element contributing to guarantee accuracy of flow prediction.

A Helmholtz potential that exhibits regions of instabilities, that is, regions in which the stability conditions [Eqs. (3) and (4)] are infringed, in a given (T, v) domain of interest contains in principle all of the required information pertinent to the single- and multiphase thermodynamics of the medium it describes. In particular, and of much significance here, it allows to perform a complete quantitative analysis of the phase equilibria of the medium. On the fluid dynamics side, it establishes the functional dependencies for pressure [Eq. (1)] and internal energy [Eq. (2)] required in the flowfield equations to proceed to the numerical solution of single-phase flows of the medium. Moreover, it provides the thermodynamic background appropriate to deal with the multiphase flows of the medium, although, in this case, composition equations must be introduced and Eqs. (1) and (2) must be properly adapted. These considerations are not peculiar to the Helmholtz potential, but are true for any equivalent fundamental relation and its associated conditions of thermodynamic stability.

III. Construction of the Thermodynamic Model

A. Introductory Considerations

As outlined earlier, the desirable thermodynamic model would, obviously, be the one whose Helmholtz potential could describe all

of the phases of the medium in the given (T, v) domain of interest. However, a century ago Planck[10] warned that "In its most complete form the characteristic equation would comprise the gaseous, liquid, and solid states simultaneously. No formula of such generality, however, has yet been established for any substance." The situation has not changed much since then, according to the more recent echo to Planck's warning from Zemansky and Dittman[11]: "It is impossible to express the complete behavior of a substance over the whole range of measured values of p, V and T by means of one simple equation." Such authoritative statements, and similar ones encountered in the literature, endorse the idea that, although theoretically useful, the all-phases embracing analytical model is bound to remain a purely ideal concept. In practice, adjacent phases and their associated transition must be studied separately, and the Helmholtz potential must be constructed analytically in a piecewise manner. Taking into account the previous teachings, our attention was motivated to concentrate towards the liquid–vapor phase transition by preliminary experimental investigations[3] carried out with liquid N_2H_4 because they revealed the presence of a substantial amount of vapor in the flow, thus indicating that solidification may occur prevalently with passage through evaporation rather then directly from the liquid.

Even considering only liquid and vapor phases as targets, there are different levels of variable difficulty from which the construction of the thermodynamic model can begin. The methods of statistical thermodynamics[12–14] certainly offer the most rigorous base, but they have the drawback of being theoretically complex and mathematically cumbersome. For the latter constraint, the methods of axiomatic thermodynamics[4–8] are undoubtedly more favorable. They are theoretically straightforward and mathematically simple, and all they require is the knowledge of the state equation $p = p(T, v)$ and of perfect-gas, constant-pressure, specific-heat data. Of course, they presuppose as done the work necessary to produce that starting-point information, and this is a major effort in itself. The specific-heat data raise no concern: They can be either measured or calculated from partition functions. The state equation calls for more attention. In principle, it could be obtained via molecular-dynamics or direct-simulation Monte Carlo calculations or from experimental investigations. In practice, the widespread preferred shortcut approach consists in the assignment of an empirical state equation, which carries a set of constants to be determined by fitting experimental evidence and/or by securing the required mathematical behavior according to arguments of physical consistency. According to Zemansky and Dittman,[11] "There have been over sixty equations of state suggested to represents only liquid, vapor, and liquid-vapor regions . . . ." Thus, there exists a rather plentiful catalog[15] of empirical state equations to choose from. Counterintuitive as it may sound, such an abundance constitutes a disadvantage because it makes more lengthy the qualification and validation processes aimed to select the state equation $p = p(T, v)$ suitable for the application of interest. An additional complication arises from the proliferation of tunable constants introduced in the empirical state equations to capture proper physical behavior in as large as possible domains of the (T, v) plane. Notwithstanding these adverse aspects, the empirical approach still offers better affordability with respect to the other mentioned alternatives when this is measured in terms of time required for model development. For this reason, it was adopted in the present study.

B. State Equation $p = p(T, v)$ and Its General Features

The model developed is founded on the state equation

$$p = RT/(v - A) - C/T^n(v + B)^2 \tag{6}$$

Equation (6) is a slightly modified version of the state equation that Planck[10] attributed to Clausius and proposed as a better performing alternative to the van der Waals state equation. The modification consists in the introduction of an exponent n to modulate the influence of the temperature on the real-gas term. There is no novelty in such an approach. In 1948, for example, Redlich and Kwong[16] did something similar in their state equation, although the temperature exponent was fixed to the value 0.5 in that case. The parameter n should be considered, in general, as a constant to be determined exactly in the same guise as the constants A, B, and C; its relevance and importance will appear clear in Sec. V. Note, however, that the more familiar van der Waals, Berthelot, and Clausius state equations are all embedded in Eq. (6) and are easily recoverable by setting, $(n = 0;\ B = 0)$, $(n = 1;\ B = 0)$, and $(n = 1)$, respectively.

The imposition of the three critical-point conditions

$$p_c = p(T_c, v_c) \tag{7}$$

$$\left(\frac{\partial p}{\partial v}\right)_T = 0 \qquad (\text{at } T_c, v_c) \tag{8}$$

$$\left(\frac{\partial^2 p}{\partial v^2}\right)_T = 0 \qquad (\text{at } T_c, v_c) \tag{9}$$

ensures the physically consistent behavior of the model at that thermodynamic point and provides a means to obtain the constants A, B, and C from the experimentally determined critical conditions p_c, v_c, and T_c. State equations with three or more constants are well suited for this purpose because Eqs. (7–9) can be matched regardless of the considered substance. On the contrary, two-constant state equations are not well predisposed in this sense because they cannot satisfy simultaneously Eqs. (7–9) in general but only under some fortuitous circumstances strongly dependent on the favorable combination of the critical conditions of the substance under consideration. The resolution of the algebraic system obtained by substituting Eq. (6) and its derivatives in Eqs. (7–9) leads to the expressions

$$A = v_c\left(1 - \frac{1}{4Z_c}\right) \tag{10}$$

$$B = -v_c\left(1 - \frac{3}{8Z_c}\right) \tag{11}$$

$$C = \frac{27}{64}\frac{R^2 T_c^{n+2}}{p_c} \tag{12}$$

where $Z_c = p_c v_c / RT_c$ represents the critical compressibility ratio. The agreed values for critical temperature and pressure are $T_c = 653.15$ K and $p_c = 14.69$ MPa, respectively. The experimental determination of the critical specific volume presents difficulties, and estimates are affected by uncertainties. Proposed values of v_c are 3.155×10^{-3} m^3/kg and 4.33×10^{-3} m^3/kg. Correspondingly, the critical compressibility ratio Z_c assumes the values 0.273 and 0.376. A detailed discussion concerning critical data of N_2H_4 and related inaccuracies is provided in Ref. 17. The positiveness of the specific covolume A sets a limit of applicability for the assumed state equation [Eq. (6)] because, taking into account Eq. (10), it implies the limitation $Z_c > \frac{1}{4} = 0.25$. Substances whose critical compressibility ratio violates such a limitation cannot be described by Eq. (6); a typical example is water with $Z_c \simeq 0.23$.

With the constants A, B, and C given by Eqs. (10–12), the assumed state equation can be conveniently recast in terms of reduced pressure $\pi = p/p_c$, temperature $\tau = T/T_c$, and specific volume $\phi = v/v_c$ to read

$$\pi = \frac{4\tau}{4Z_c(\phi - 1) + 1} - \frac{1}{\tau^n}\frac{27/4}{[4Z_c(\phi - 1) + 3/2]^2} \tag{13}$$

The change of variable

$$\varphi = 4Z_c(\phi - 1) + 1 \tag{14}$$

shifts the origin of the nondimensional specific-volume axis in correspondence to the covolume vertical asymptote and transforms Eq. (13) into the interesting form

$$\pi = \frac{4\tau}{\varphi} - \frac{1}{\tau^n}\frac{27/4}{(\varphi + 1/2)^2} \tag{15}$$

Equation (15) possesses the desirable feature of being freed from the presence of the critical compressibility ratio. As it will be seen in the sequel, such a feature is passed on to all nondimensional thermodynamic properties. Critical-data dependency is relegated exclusively

to Eq. (14), which, when resolved for the non-dimensional variable $\phi = v/v_c$, represents a scaling law to determine the dimensional specific volume. In the case of N_2H_4, this fortunate mathematical circumstance confines, to a certain extent, the potential harm of critical-data inaccuracies, but, of course, it in no way diminishes the importance of the necessity to remove them. The only channel left in Eq. (15) through which the nature of the substance can manifest itself is the exponent n. Typical isotherms are shown in Fig. 1. Figure 1 emphasizes the existence of a characteristic isotherm ($\tau = \tau_t$) that is tangent to the φ axis. Negative-pressure ranges appear below the tangent isotherm. The range limits are obtained analytically as

$$\varphi_{\mathrm{np}} = \tfrac{1}{2}\left[\tfrac{27}{16}(1/\tau^{n+1})\left(1 \mp \sqrt{1 - \tfrac{32}{27}\tau^{n+1}}\right) - 1\right] \qquad (16)$$

by setting $\pi = 0$ in Eq. (15); negative and positive signs correspond to left and right limits, respectively. The dependence on the reduced temperature expressed by Eq. (16) is shown by curve i in Fig. 2 for $n = 0.7$. All states characterized by negative pressure reside in the portion of plane below that curve. The tangent-isotherm reduced temperature is the one for which the argument of the squared root in Eq. (16) vanishes; this occurs when

$$\tau_t = \left(\tfrac{27}{32}\right)^{1/(n+1)} \qquad (17)$$

Correspondingly, the tangency point is located at $\varphi_{\mathrm{np,l}} = \varphi_{\mathrm{np,r}} = \frac{1}{2}$, that is, where the specific volume attains the mean value between specific covolume and critical specific volume. The existence of negative-pressure ranges is a somewhat unusual feature of state equations similar to van der Waals's that is rarely discussed in the literature.[18,19] With reference to Fig. 2, the probable reasons explaining why it apparently does not represent a concern are 1) the theoretically predicted liquid–vapor transitions (curve iii) always take place in the positive-pressure region (above curve i), cutting out, in so doing, the isotherm portions trespassing into negative-pressure regions (see Fig. 1) and 2) the majority of the negative-pressure states is contained in the domain of the unstable states (below curve ii). Nevertheless, this aspect deserves careful attention when the metastable states of the liquid have to be dealt with because the latter overlap, although in a reduced manner, with negative-pressure states.

The minima and maxima of the isotherms shown in Fig. 1 constitute other characteristic points of interest because they represent the terminal points of the unstable-state ranges, that is, the intervals in which the second stability condition [Eq. (4)] is infringed. The corresponding coordinates (π_m, φ_m) and (π_M, φ_M) can be found from the numerical solution of

$$\left(\frac{\partial \pi}{\partial \varphi}\right)_\tau = -\frac{4\tau}{\varphi^2} + \frac{1}{\tau^n}\frac{27/2}{(\varphi + 1/2)^3} = 0 \qquad (18)$$

A typical spinodal line produced by Eq. (18), with $n = 0.7$, is represented by curve ii in Fig. 2; the unstable states reside in the area below this curve. The dashed portion of the left branch emphasizes the minima that fall in the negative-pressure region.

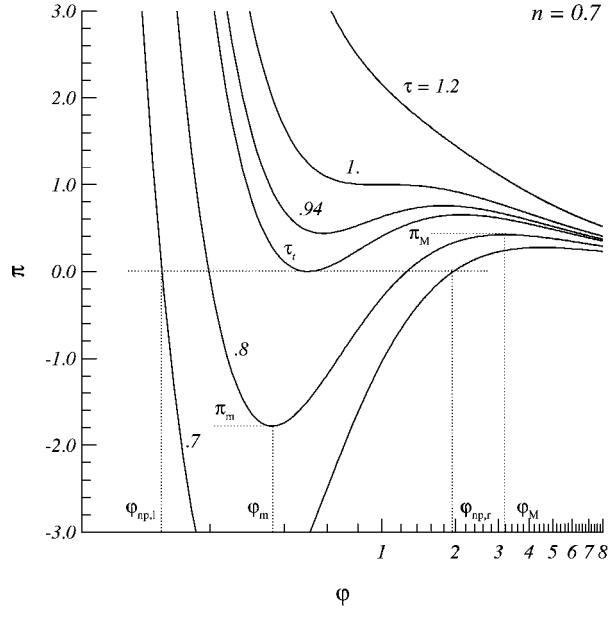

Fig. 1 Typical isotherms of the nondimensional modified Clausius state equation [Eq. (15)].

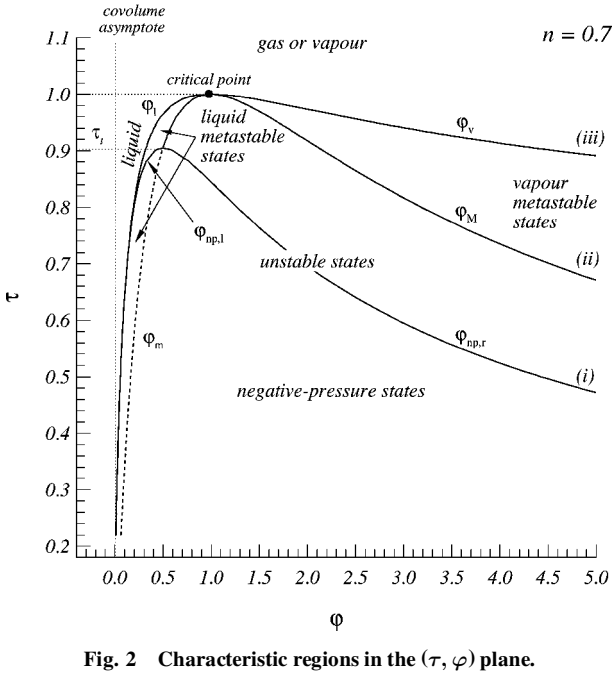

Fig. 2 Characteristic regions in the (τ, φ) plane.

C. Fundamental Relation $f = f(T, v)$

The construction of the fundamental relation $f(T, v)$ from an assigned state equation $p(T, v)$ and theoretical information about the constant-volume specific heat is conceptually straightforward. The state equations in the Helmholtz-potential formulation turn out to be entropy and pressure

$$\left(\frac{\partial f}{\partial T}\right)_v = -s(T, v) \qquad (19)$$

$$\left(\frac{\partial f}{\partial v}\right)_T = -p(T, v) \qquad (20)$$

The availability of Eq. (6) leads, thus, via the integration of the Maxwell relation

$$\left(\frac{\partial s}{\partial v}\right)_T = \left(\frac{\partial p}{\partial T}\right)_v \qquad (21)$$

to the following expression of the entropy:

$$s(T, v) = \psi(T) + R\,\ln(v - A) - \frac{nC}{T^{n+1}(v + B)} \qquad (22)$$

The unknown function $\psi(T)$ in Eq. (22) needs, of course, to be determined; specific-heat data can be used for this purpose. The expression of the constant-volume specific heat follows from Eq. (22) according to the definition holding in the Helmholtz-potential formulation

$$c_v = T\left(\frac{\partial s}{\partial T}\right)_v = T\frac{\mathrm{d}\psi}{\mathrm{d}T} + \frac{n(n+1)C}{T^{n+1}(v + B)} \qquad (23)$$

The second term on the right-hand side of Eq. (23) features a specific-volume dependence, and at any given temperature, it expectedly decreases when the specific volume becomes large, that is,

when the behavior of the vapor tends toward that of a perfect gas. Therefore, reasons of physical consistency oblige setting

$$T\frac{\mathrm{d}\psi}{\mathrm{d}T} = \lim_{v\to\infty} c_v = c_{v;\mathrm{pg}} = \Phi(T) \tag{24}$$

to secure the correct asymptotic behavior. Equation (24) identifies the derivative of the unknown function $\psi(T)$ in terms of the perfect-gas, constant-volume, specific heat, which is well known to be a function $\Phi(T)$ of the sole temperature; thus,

$$\frac{\mathrm{d}\psi}{\mathrm{d}T} = \frac{\Phi(T)}{T} \tag{25}$$

Values of the function $\Phi(T)$ calculated from partition-function methods[20–22] are shown in Fig. 3. Some divergences among the data are evident, due to differences in energy levels, molecular constants, and cut-off criteria used in the partition-function summations.[17] The data provided by Gurvich et al.[22] have been interpolated according to the polynomial form

$$\frac{\Phi(T)}{R} = \sum_{k=0}^{6} a_k \left(\frac{T}{T_c}\right)^k \tag{26}$$

The coefficients a_k are listed in Table 1. The accuracy of Eq. (26) is shown by the solid line in Fig. 3. After the formal integration of Eq. (25), the expression of the entropy [Eq. (22)] becomes

$$s(T,v) = K_1 + \int \frac{\Phi(T)}{T}\,\mathrm{d}T + R\,\ell n(v-A) - \frac{nC}{T^{n+1}(v+B)} \tag{27}$$

The Helmoltz potential follows from the integration of Eqs. (19) and (20) taking into account Eqs. (6) and (27). It reads

Table 1 Coefficients for interpolating the function $\Phi(T)$

	a_k	
k	Temperature range, K 100–600	Temperature range, K 600–6000
0	2.308406668124E+00	1.360153870060E+00
1	9.577413069779E+00	9.694388016457E+00
2	−4.278518667362E+01	−3.555174260821E+00
3	1.435137405516E+02	7.585461810897E−01
4	−2.080151427938E+02	−9.459603992578E−02
5	1.394963154578E+02	6.359914582051E−03
6	−3.588688076504E+01	−1.774004796525E−04

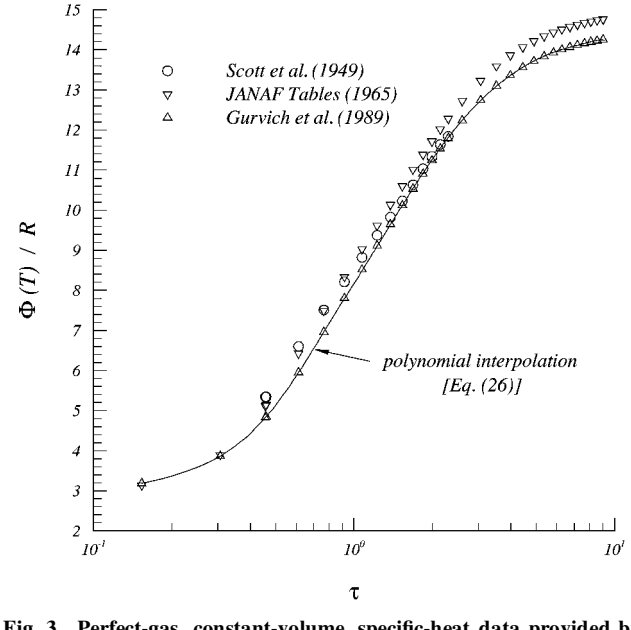

Fig. 3 Perfect-gas, constant-volume, specific-heat data provided by Scott et al.,[20] JANAF tables,[21] and Gurvich et al.[22]

$$f(T,v) = K_2 - K_1 T - \int \mathrm{d}T \int \frac{\Phi(T)}{T}\,\mathrm{d}T - RT\,\ell n(v-A) - \frac{C}{T^n(v+B)} \tag{28}$$

Any thermodynamic information that can be possibly asked about the developed model is contained in Eq. (28). For example, the substitution of Eq. (28) into Eq. (2) provides the internal energy,

$$u = K_2 + \int \Phi(T)\,\mathrm{d}T - \frac{(n+1)C}{T^n(v+B)} \tag{29}$$

The enthalpy follows from the general definition $h = u + pv$ and reads

$$h = K_2 + \int \Phi(T)\,\mathrm{d}T + \frac{RTv}{(v-A)} - \frac{(n+1)C}{T^n(v+B)} - \frac{Cv}{T^n(v+B)^2} \tag{30}$$

The Mollier diagram can be easily constructed from Eqs. (6), (27), and (30) by using temperature and specific volume as parameters.

IV. Other Available Thermodynamic Models

Thermodynamic models of N_2H_4 have been proposed by Haws and Harden,[23] Das and Kuloor,[24] Tsykalo et al.,[25] and Barragan et al.[26,27]

Haws and Harden's model[23] is based on the particularization to N_2H_4 of the generic virial-expansion state equation

$$p = \frac{RT}{v-b} + \frac{A_2 + B_2T + C_2\exp(-xT/T_c)}{(v-b)^2} + \frac{A_3 + B_3T + C_3\exp(-xT/T_c)}{(v-b)^3} + \frac{A_4}{(v-b)^4} + \frac{B_5T}{(v-b)^5} \tag{31}$$

proposed by Martin and Hue[28] and Martin et al.[29] Das and Kuloor[24] slightly modified Eq. (31) by adding the factor $C_5\exp(-xT/T_c)$ to the numerator B_5T of the last term on the right-hand side. The coefficients appearing in Eq. (31) as given by Haws and Harden and Das and Kuloor are collected in Tables 2 and 3, respectively. Particular attention should be paid to physical units. In particular, Haws and Harden give the value 10.7315 for the universal gas constant but without indicating the corresponding physical units; these turn out to be psi · ft^3 · R^{-1} · (g · lbm^{-1}). Thus, the molar mass of N_2H_4 (mol wt in Table 2) must be expressed in grams to obtain the value of the gas constant R consistent with Eq. (31). Moreover, one has to assume that the undeclared units of the coefficients following the critical temperature T_c in Table 2 and 3 are consistent with those of pressure, temperature, and specific volume adopted by the mentioned authors and listed in Table 4.

The behavior of Eq. (31) in nondimensional form and with the coefficients of Table 2, is shown in Fig. 4. The isotherms above $\tau = 0.70$ present the expected trend; those below $\tau = 0.70$ fail to

Table 2 Coefficients for Eq. (31) proposed by Haws and Harden[23]

Coefficient	Value
R	10.7315/mol wt
b	0.0299451 ft^3 · lbm^{-1}
x	8.00000
T_c	1175.69 R
A_2	−32.21898
B_2	0.00294549
C_2	−1171.2876
A_3	0.869588
B_3	0.16838487×10^{-3}
C_3	46.250721
A_4	-0.202100×10^{-1}
B_5	0.12899897×10^{-6}

provide a satisfactory representation of the pressure dependence on specific volume. Nevertheless, Haws and Harden[23] explicitly declare the temperature range of their calculations to be between 273.15 and 760 K (τ between 0.42 and 1.16). It is, therefore, somewhat puzzling to understand how these authors could produce the N_2H_4 Mollier diagram reported in Fig. 1 of Ref. 23. Of course, a possible explanation could be the presence of unknown mistakes in the values of the coefficients they provide (see Table 2). On the other hand, the fact that a situation similar to the one represented in Fig. 4 exists also with the Das and Kuloor's modification[24] of Eq. (31) and with the coefficients of Table 3 makes the erroneous-coefficient conjecture somewhat weak and points into the direction of questioning the mathematical structure of Eq. (31). At any rate, this matter was not investigated further and, for the time being, it remains unresolved. This unclear aspect notwithstanding, it is possible to develop a theoretical model from the virial-expansion state equation [Eq. (31)] proposed by Haws and Harden by following the same procedure described in Sec. III.C. The resulting Helmholtz potential reads

$$f(T,v) = K_2 - K_1 T - \int \mathrm{d}T \int \frac{\Phi(T)}{T}\,\mathrm{d}T - RT\,\ln(v-b) + \frac{A_2 + B_2 T + C_2 \exp(-xT/T_c)}{v-b} + \frac{A_3 + B_3 T + C_3 \exp(-xT/T_c)}{2(v-b)^2} + \frac{A_4}{3(v-b)^3} + \frac{B_5 T}{4(v-b)^4} \tag{32}$$

Tsykalo et al.[25] were mainly interested in the thermodynamic properties of N_2H_4 in the compressed-gas region. They based their model on the state equation

$$p = RT/[v - b(T)] \tag{33}$$

for the vapor phase and treated the liquid separately and as incompressible. Thus, for the reasons discussed in Sec. II, their model does not appear suitable for implementation in a fluid dynamics context. The paper of Tsykalo et al. is difficult to interpret; the method they used to determine the covolume function $b(T)$ is not completely clear. At any rate, they determined it numerically (see Table 2 of Ref. 25) and then supplied the following interpolation polynomial:

$$b(T) = -0.0104668 + 0.2649938X - 0.8832357X^2 + 0.6849432X^3 - 0.2101736X^4 \tag{34}$$

with $X = 10^3/T(\mathrm{K}^{-1})$. The covolume units in Eq. (34) are cubic centimeter per mole. Concerning aspects of thermodynamic stability, the constant-volume specific heat compatible with Eq. (33) can be easily obtained by following the same technique described in Sec. III.C; it reads

$$c_v = \Phi(T) - RTb''/(v-b) - [Rb'/(v-b)][1 + Tb'/(v-b)] \tag{35}$$

In Eq. (35), the prime denotes differentiation with respect to temperature. The signs of the derivatives are easily obtained by plotting the data provided in Table 2 of Ref. 25 vs temperature; they turn out to be $b' > 0$ and $b'' < 0$. Thus, the last term on the right-hand side always subtracts to the preceding ones and, therefore, there could be regions of the (T, v) plane in which the first stability rule [Eq. (3)]

Table 3 Coefficients for Eq. (31) and the additional term $C_5 e^{-xT/T_c}$ proposed by Das and Kuloor[24]

Coefficient	Value
b	$0.05971 \cdot \mathrm{mol}^{-1}$
x	5.475
T_c	653.15 K
A_2	−8.5158
B_2	0.126×10^{-2}
C_2	-0.5988×10^{-2}
A_3	0.5312
B_3	0.6045×10^{-4}
C_3	4.8052
A_4	-0.0221×10^{-1}
B_5	0.5100×10^{-6}
C_5	-0.4003×10^{-3}

Table 4 Pressure, temperature, and specific-volume units used by Haws and Harden and Das and Kuloor in relation to Eq. (31)

Parameter	Haws and Harden[23]	Das and Kuloor[24]
p	psi	atm
T	°R	K
v	$\mathrm{ft}^3 \cdot \mathrm{lbm}^{-1}$	$1 \cdot \mathrm{mol}^{-1}$

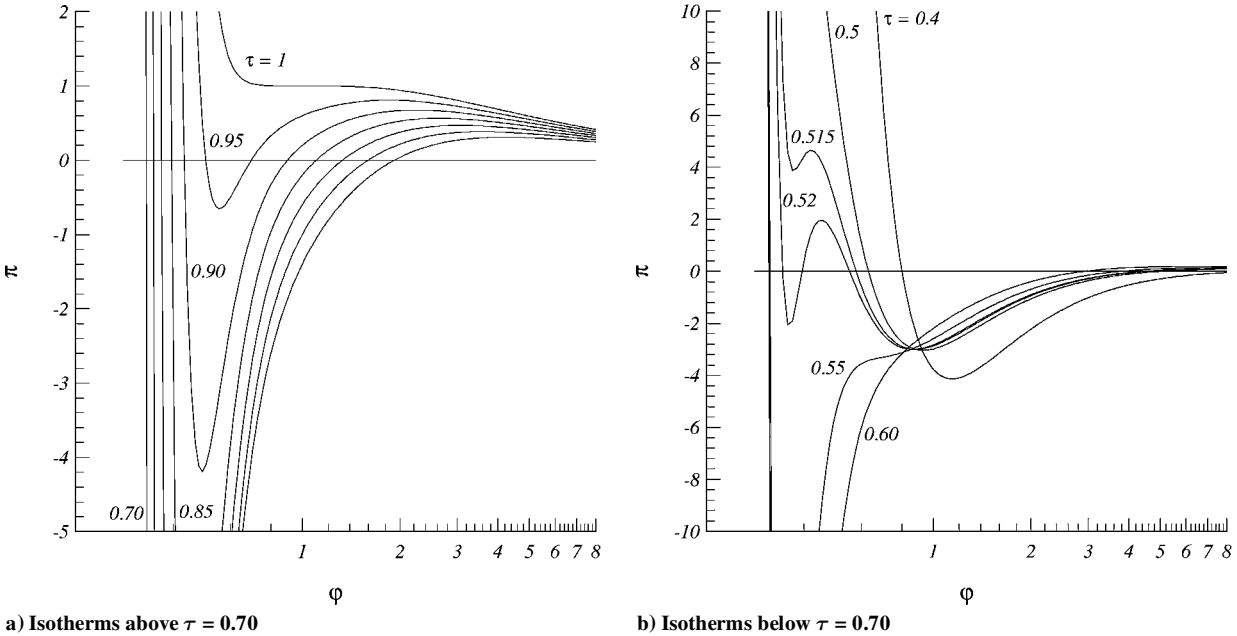

a) Isotherms above $\tau = 0.70$ **b) Isotherms below $\tau = 0.70$**

Fig. 4 Behavior of the virial-expansion state equation [Eq. (31)] proposed by Haws and Harden.[23]

might be infringed. However, Tsykalo et al. did not consider whether or not this circumstance could be exploited to characterize a possible phase change. The isothermal speed of sound descends from the substitution of Eq. (33) in Eq. (5)

$$\left(\frac{\partial^2 f}{\partial v^2}\right)_T = \frac{a_N^2}{v^2} = \frac{RT}{[v - b(T)]^2} \tag{36}$$

and remains always positive. Thus, the second stability rule [Eq. (4)] is never infringed in the whole (T, v) plane.

Barragan et al.[26,27] constructed their model on the Peng–Robinson state equation. The details of their method are described in Ref. 26. In brief, they used the correlation

$$\log p_v = 60.878 - (3880.3/T) - 20.575 \log T + 15.585 \times 10^{-3} T - 5.0525 \times 10^{-6} T^2 \tag{37}$$

provided by Yaws[30] to reproduce experimental vapor-pressure data (in millimeters mercury) and, by enforcing the equilibrium criterion of fugacity equality, they tuned on those data, over the range from 288 up to 653 K, the several parameters involved in the definition of the temperature function [$a(T)$ in the notation of Ref. 26] appearing at the numerator of the real-gas term in the Peng–Robinson state equation. As Barragan et al. themselves inform in Ref. 26, the accuracy of their procedure is satisfactory between normal-boiling and critical temperatures, but deviations from the fugacity-equality condition appear below the normal boiling point (see Fig. 2 in Ref. 26). Unfortunately, it appears that these authors did not carry out a phase-equilibrium theoretical calculation, as described in Sec. V, to see how the fugacity-equality deviations translate in terms of accuracy loss on the vapor pressure. In Table 6 of Ref. 27, they provide vapor pressure estimated from Eq. (37) and specific volume, internal energy, enthalpy, and entropy of saturated liquid and vapor calculated from their Peng–Robinson generated model.

V. Liquid–Vapor Phase Equilibrium

The complete characterization of the equilibrium among the different phases of a substance is an elegant application of the general principle of thermodynamic equilibrium formulated in terms of either energy minimization or entropy maximization. Planck,[10] for example, based his treatment on the entropy-maximization formulation of the principle, but alternative approaches have been presented and, in general, the subject has been widely dealt with in the literature.[4–6,11,31–34] In the absence of surface effects of chemical reactions at the phase interfaces, and when volume is the sole deformation coordinate characterizing the thermodynamic behavior of solid phases, the basic equations governing the equilibrium express the continuity of temperature, pressure, and chemical potential among the phases. In the case of liquid–vapor transition, these equations read

$$T_l = T_v \quad (= T) \tag{38}$$

$$p(T, v_l) = p(T, v_v) \tag{39}$$

$$\mu(T, v_l) = \mu(T, v_v) \tag{40}$$

Equations (38–40) are cast in the formalism of the Helmholtz-potential formulation, and the thermal equilibrium expressed by Eq. (38) has already been enforced in Eqs. (39) and (40). The latter constitute an algebraic system for the unknown saturated-liquid and vapor specific volumes v_l and v_v. After these have been determined, the saturation pressure follows from

$$p_v = p(T, v_v) = p(T, v_l) = p_l \tag{41}$$

The chemical potential relative to the model constructed in Sec. III can be obtained in a variety of alternative and, obviously, equivalent manners. The most convenient one in the present context is that which takes advantage of its coincidence with the Gibbs potential and relies on the Legendre-transformation definition of the latter

$$\mu = g = f + pv \tag{42}$$

The substitution of Eqs. (6) and (28) into Eq. (42) yields

$$\mu(T, v) = K_2 - K_1 T - \int \mathrm{d}T \int \frac{\Phi(T)}{T}\,\mathrm{d}T - RT\,\ell n(v - A) + RT\frac{v}{v - A} - \frac{C}{T^n(v + B)} \cdot \frac{2v + B}{v + B} \tag{43}$$

The temperature-only dependent part

$$\hat{\mu}(T) = K_2 - K_1 T - \int \mathrm{d}T \int \frac{\Phi(T)}{T}\,\mathrm{d}T \tag{44}$$

of the chemical potential [and, consequently, the integration constants K_1, K_2 and the function $\Phi(T)$] plays no role in the characterization of the phase equilibrium because it disappears after substitution into Eq. (40). It is, therefore, only the part featuring specific-volume dependency

$$\tilde{\mu}(T, v) = -RT\,\ell n(v - A) + RT\frac{v}{v - A} - \frac{C}{T^n(v + B)} \cdot \frac{2v + B}{v + B} \tag{45}$$

that controls the phase equilibrium together with the assumed state equation [Eq. (6)]. When account is taken of Eq. (6), Eqs. (10–12) and Eq. (43), and use is made of the reduced variables π, τ, and ϕ with the additional change of variable given by Eq. (14), the system composed by Eqs. (39) and (40) turns, after simple algebraic manipulations, into the following explicit nondimensional form:

$$\frac{4\tau}{\varphi_l} - \frac{1}{\tau^n}\frac{27/4}{(\varphi_l + 1/2)^2} = \frac{4\tau}{\varphi_v} - \frac{1}{\tau^n}\frac{27/4}{(\varphi_v + 1/2)^2} \tag{46}$$

$$\tau\,\ell n\varphi_l + \frac{27}{8\tau^n}\frac{\varphi_l + 1/4}{(\varphi_l + 1/2)^2} = \tau\,\ell n\varphi_v + \frac{27}{8\tau^n}\frac{\varphi_v + 1/4}{(\varphi_v + 1/2)^2} \tag{47}$$

to be solved for the unknowns φ_l and φ_v. The reduced saturation pressure π_v is then obtained by substituting either φ_l or φ_v in Eq. (15). The solution of Eqs. (46) and (47) is shown in Fig. 5 for $n = 0.7$ at $\tau = 0.92$. Figure 5 shows the corresponding isotherm [Eq. (15)] overlaid on the diagram of the nondimensional function

$$\mu^* = \tau\,\ell n\varphi + \frac{27}{8\tau^n}\frac{\varphi + 1/4}{(\varphi + 1/2)^2} \tag{48}$$

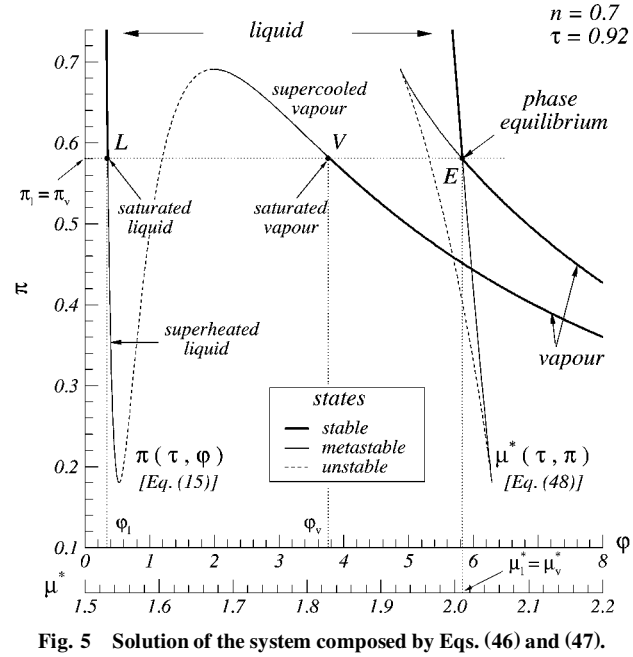

Fig. 5 Solution of the system composed by Eqs. (46) and (47).

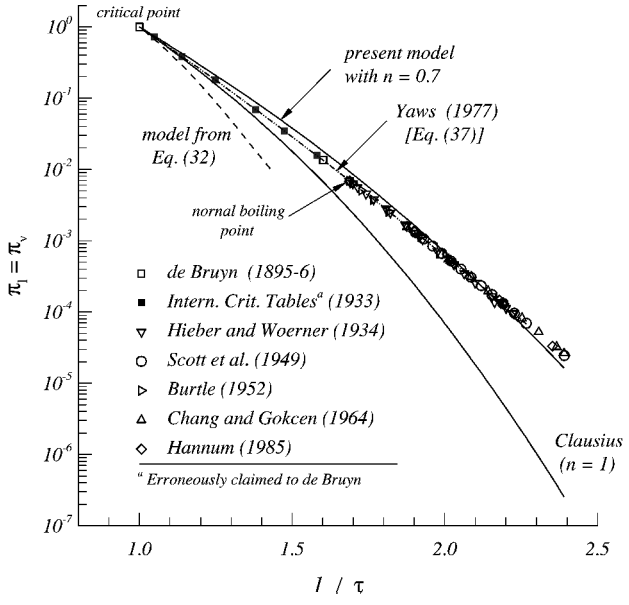

Fig. 6 Liquid–vapor phase equilibrium; experimental saturation curve and theoretical predictions.

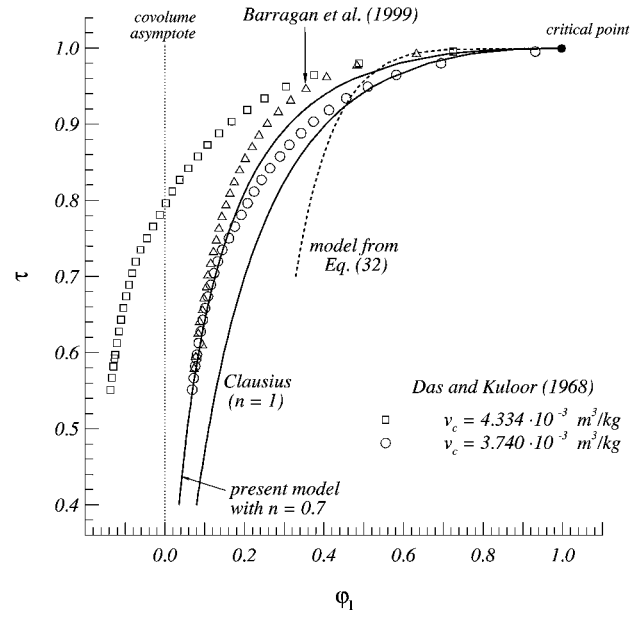

a) Saturated liquid

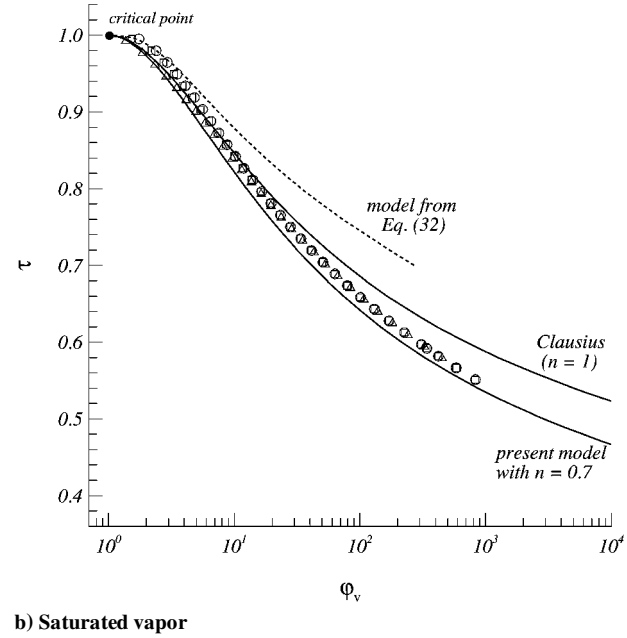

b) Saturated vapor

Fig. 7 Liquid–vapor phase equilibrium; theoretical predictions of the saturated reduced shifted specific volumes.

intervening in Eq. (47). This function is plotted vs reduced pressure to evidence the characteristic closed-loop shape[5,6] revealing the phase-equilibrium point E as the intersection of the liquid and vapor branches. In correspondence to this point, the saturated-liquid and -vapor points L and V can be identified on the isotherm. The quantitative determination of the associated coordinates φ_l and φ_v and $\pi_l = \pi_v$ requires a numerical algorithm. Note that the critical compressibility ratio does not appear in Eqs. (46) and (47) and, therefore, it does not affect their solution. This means also that the liquid–vapor saturation curve produced by these equations is immune from the uncertainties about the critical data of N_2H_4 mentioned in Sec. III.B.

Liquid–vapor equilibrium results for different theoretical models are compared in Figs. 6 and 7. Figure 6 shows theoretical predictions of the N_2H_4 saturation curve superposed to experimental data[20,35–41] from $\tau \simeq 0.42$ ($T \simeq 273.15$ K) up to the critical point. Given the fugacity-equality match shown in Fig. 2 of Ref. 26, the correlation [Eq. (37); dash–dot–dot line] proposed by Yaws[30] is also representative of the excellent prediction capability featured between critical and normal-boiling points by the model developed by Barragan et al.[26,27] However, such a representativeness cannot be assumed, and its extent should be verified below the normal boiling point due to the fugacity-equality deviations produced by the model below that temperature (see Sec. IV). The model (dashed line) derived from Haws and Harden's virial expansion can be used only in the reduced-temperature range between $\tau = 0.7$ and the critical point for the reasons described in Sec. IV. Even in this restricted range, the predicted curve lies appreciably below the experimental data. In turn, the present model offers a better approximation with respect to the previous one, but does not perform as accurately as the Barragan et al. model above the normal boiling point. The value of the exponent $n = 0.7$ was simply obtained by a trial-and-error procedure aimed to match as satisfactorily as possible the experimental data in the reduced-temperature range (τ between 0.42 and 0.5) of concern to the SCA application. There is indeed a more exact way to estimate the exponent n, and there will be occasion to come back to this aspect in the course of the discussion about the vaporization enthalpy (see Sec. VI.A).

Figure 7 shows the saturated reduced shifted specific volumes. Experimental data are not available in this case and the sole possibility of comparison is offered by similar data calculated by Das and Kuloor[24] in 1968 (square and circle symbols) and, more recently, by Barragan et al.[26,27] (triangle symbols). The reader is warned, however, that the method followed by Das and Kuloor to estimate the saturated-liquid and -vapor molar specific volumes is not free from inaccuracies. The latter are described and commented on in Ref. 17. Figure 7a yields full evidence of the effect produced by the uncertainties about the critical specific volume. The square symbols represent Das and Kuloor's data made nondimensional with the value $v_c = 4.334 \times 10^{-3}$ m^3/kg obtained from the molar critical specific volume (0.1389 l/mol) originally supplied by the same authors. The data are seen to cross the boundary set by the covolume asymptote of the present model. The circle symbols represent the same data but made nondimensional with the value $v_c = 3.740 \times 10^{-3}$ m^3/kg. The justification for such a choice will appear clear when discussing the validation procedure of the present model with respect to liquid-density experimental data (see Sec. VI.B). With the latter figure of v_c, Das and Kuloor's data align more satisfactorily with the results predicted by the present model. The same effect is also perceptible in the vicinity of the critical point on the vapor side (see Fig. 7b) and vanishes when φ_v increases, as expected from Eq. (14). Given the behavior of Das and Kuloor's data, those calculated by Barragan et al. have been made non-dimensional only with the value $v_c = 3.740 \times 10^{-3}$ m^3/kg. On the liquid side (see Fig. 7a), the

predictions from Barragan et al. and the present models disagree in the vicinity of the critical point and converge at lower temperatures. The situation turns out to be the opposite on the vapor side (see Fig. 7b): The two models agree near the critical point, but they diverge at lower temperatures, with the Barragan et al. data superposing those of Das and Kuloor. The results predicted by the model derived from Haws and Harden's virial expansion are represented by the dashed curves. They are relative to $v_c = 4.335 \times 10^{-3}$ m^3/kg obtained from the critical density ($\rho_c = 14.4$ lbm/ft^3) originally supplied by the same authors.

VI. Model-Validation Procedures

A. Vaporization Enthalpy

The expression of the vaporization enthalpy $\Delta h_{\text{vap}} = h_v - h_l$ for the present model is obtained from Eq. (30) evaluated in correspondence to the solution of the system composed by Eqs. (39) and (40). In nondimensional form it reads

$$\frac{\Delta h_{\text{vap}}}{RT_c} = \tau\, \ell n \frac{\varphi_v}{\varphi_l} + \frac{27n}{16\tau^n} \frac{\varphi_v - \varphi_l}{(\varphi_v + 1/2)(\varphi_l + 1/2)} \tag{49}$$

Results predicted from Eq. (49) are compared with data published from other authors[1,20,24,38,42,43] and with those calculated by Barragan et al.[26,27] in Fig. 8. The methods used to derive the former data have been thoroughly described and discussed in Ref. 17. It is sufficient here to mention that the widespread belief that considers the data in question to be of experimental nature turns out to be unfounded. Thus, the disagreement existing between them and the theoretical curve predicted by the present model does not necessarily reflect an inaccuracy on the model's side.

To put this aspect in clear perspective, consider the method used by Hieber and Woerner.[38] These authors estimated the vaporization enthalpy from the approximated formula

$$\Delta h_{\text{vap}} \simeq R[T_1 T_2/(T_2 - T_1)]\, \ell n \left(p_{v_2}/p_{v_1}\right) \tag{50}$$

Equation (50) is applicable 1) sufficiently far away from the critical point, 2) if the vapor behaves as a perfect gas, and 3) if the temperature interval $[T_1, T_2]$ is sufficiently small so that the vaporization enthalpy remains practically constant within it. The value of Δh_{vap} returned from Eq. (50) is attached to the temperature $(T_2 + T_1)/2$. Hieber and Woerner complemented Eq. (50) with their experimentally determined saturation-pressure data. Some of these are reported in Table 5; those marked with a label in the leftmost column constitute the selection adopted by those authors to be used in combination

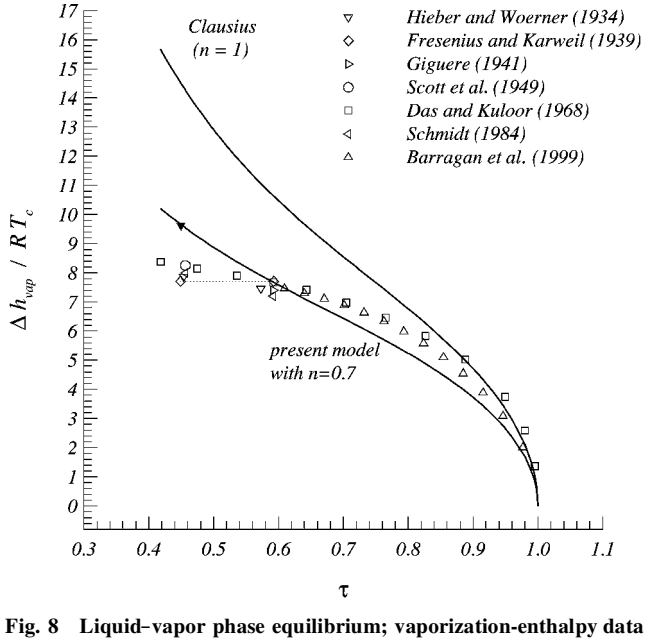

Fig. 8 Liquid–vapor phase equilibrium; vaporization-enthalpy data from various authors and theoretical predictions.

Table 5 Liquid N_2H_4 vapor pressure measured by Hieber and Woerner[38]

Experimental point	Original units		SI units	
	t, °C	p_v, mmHg	T, K	p_v, Pa
(i-1)	20.21	10.4	293.36	1.387×10^3
	20.60	10.7	293.75	1.427×10^3
(i-2)	26.02	14.6	299.17	1.947×10^3
(ii-1)	88.20	308.8	361.35	4.117×10^4
(ii-2)	114.15	760.0	387.30	1.013×10^5

Table 6 Molar vaporization enthalpy estimated by Hieber and Woerner[38]

Experimental point	Original units		SI units	
	t, °C	$M\Delta h_{\text{vap}}$, kcal · mol^{-1}	T, K	$M\Delta h_{\text{vap}}$, J · mol^{-1}
(i)	23.1	10.20	296.25	42705
(ii)	101.0	9.67	374.15	40486

with Eq. (50). The corresponding results are listed in Table 6 and are represented by the open down-triangle symbols in Fig. 8; the difference from the theoretical curve produced by Eq. (49) is evident. However, if the experimental point (i-2) is replaced with the one in the second row of Table 5, the resulting vaporization enthalpy (12.48 kcal · mol^{-1} or 52,245 J · mol^{-1}; $\Delta h_{\text{vap}}/RT_c \simeq 9.6$) turns out to be in full agreement with the theoretical prediction of the present model, as the solid down-triangle symbol in Fig. 8 clearly indicates. This simple test outlines the underlying weakness of the Hieber and Woerner's method. This weakness originates from the a priori unawareness concerning the consistency of the temperature intervals at which saturation-pressure measurements are carried out with the assumption of negligible variations of the vaporization enthalpy.

The Barragan et al.[26,27] results turn out to be in between the predictions from Das and Kuloor[24] and from the present models in the vicinity of the critical point; the tendency to agree with Das and Kuloor's data at lower temperatures is evident.

The knowledge of the vaporization enthalpy permits the determination of the slope of the liquid–vapor saturation curve in the (p, T) plane via the Clausius–Clapeyron equation

$$\frac{\mathrm{d}p_v}{\mathrm{d}T} = \frac{\Delta h_{\text{vap}}}{T(v_v - v_l)} \tag{51}$$

Equation (51) offers, in principle, the possibility of an exact method to determine the exponent n. When Eq. (49) is taken into account, the equation can be cast in the following nondimensional form:

$$\frac{\mathrm{d}\pi_v}{\mathrm{d}\tau} = 4\frac{\ell n(\varphi_v/\varphi_l)}{\varphi_v - \varphi_l} + \frac{27n/(4\tau^{n+1})}{(\varphi_v + 1/2)(\varphi_l + 1/2)} \tag{52}$$

and evaluated at the critical point ($\tau = 1$, $\varphi_v = \varphi_l = 1$) to yield

$$\left[\frac{\mathrm{d}\pi_v}{\mathrm{d}\tau}\right]_{\tau=1} = 4 + 3n \tag{53}$$

The mathematical indeterminacy of the first term on the right-hand side of Eq. (52) when $\tau \to 1$ does not constitute a problem because

$$\lim_{\tau\to 1} \frac{\ell n(\varphi_v/\varphi_l)}{\varphi_v - \varphi_l} = \lim_{\tau\to 1} \frac{\ell n[1 + (\varphi_v - \varphi_l)/\varphi_l]}{\varphi_v - \varphi_l} = \lim_{\tau\to 1} \frac{1}{\varphi_l} = 1$$

Thus, if the slope $(\mathrm{d}\pi_v/\mathrm{d}\tau)_{\tau=1}$ is known experimentally, the exponent n can be straightforwardly obtained from Eq. (53). Unfortunately, the feasibility of this approach is hindered by the unavoidable experimental difficulties that arise at the moment of performing sufficiently accurate measurements of the saturation curve in the vicinity of the critical point. Even the use of an experimental vapor-pressure interpolating function does not help because, as correctly asserted by Reid et al.,[44] "An element of uncertainty is introduced

in using any analytical vapor pressure-temperature equation to obtain accurate values of slopes dP_{vp}/dT. The constants in the equation may be optimum for correlating vapor pressures, but it does not necessarily follow that these same constants give the best fit for computing slopes" (see page 219 of Ref. 44, P_{vp} corresponds to p_v).

B. Density of the Liquid Phase

The density of liquid N_2H_4 as a function of temperature at a given pressure is obtained by inverting Eq. (14) into the form

$$\rho/\rho_c = (v/v_c)^{-1} = [1 + (\varphi - 1)/4Z_c]^{-1} \tag{54}$$

and by solving the nondimensional state equation [Eq. (15)] for the unknown φ (left root). In this regard, particular attention must be paid to dealing correctly with the metastable states of the liquid phase. The presence of the critical compressibility ratio on the right-hand side of Eq. (54) makes inescapable the necessity to confront the uncertainties, mentioned in Sec. III.B, affecting the value of the critical specific volume. This is clearly shown in Fig. 9, which shows the comparison between experimental data collected from the literature[35,36,41,45–55] and the predictions of the present model. Note that most of the cited references do not provide sufficient information regarding the pressure at which the measurements were taken.[17] Only Hough et al.[51] state unambiguously that their experiments were carried out under atmospheric pressure. The calculations relative to the present model have been carried out systematically at atmospheric pressure ($\pi \simeq 0.00689$). Figure 9a shows the situation corresponding to $v_c = 4.33 \times 10^{-3}$ m^3/kg: The experimental data fall below the theoretical curve. Figure 9b shows the one relative to $v_c = 3.155 \times 10^{-3}$ m^3/kg. In this case, the layout turns out to be the opposite to the preceding one: The theoretical curve noticeably overshoots the experimental data. Such a marked influence of the critical specific volume suggests that there should be a value for it, between the two extremes provided by the literature (those of Figs. 9a and 9b), according to which the theoretical curve might satisfactorily match the experimental data. Indeed, with the exponent n fixed to 0.7 (see Sec. V), a simple trial-and-error procedure leads to $v_c = 3.740 \times 10^{-3}$ m^3/kg. As shown in Fig. 10, experimental data and theoretical prediction compare well in correspondence to such a value. The divergence from the Ahlert et al. data[54] (circles) does not represent a concern because the latter data appear to have been measured under nonisobaric conditions. Ahlert et al., in fact, mention briefly that their data correspond to different pressure levels with a maximum of 12 atm (1.2159×10^6 Pa) at 449.83 K, or $\tau \simeq 0.69$ (rightmost circle in Figs. 9 and 10). The satisfactory match shown in Fig. 10 makes unrefutable that the present model performs well in combination with the scale factor $v_c = 3.740 \times 10^{-3}$ m^3/kg rather than with the values available from the literature. However, this positive feature is certainly not sufficient to purport the idea that such a value represents the correct value of the critical specific volume and that the relative uncertainties have been finally resolved. Obviously, this is an aspect that deserves deeper thought and in which the possibility of N_2H_4 decomposition in the vicinity of the critical point[1,56,57] must necessarily be taken into adequate account. The matter, however, is beyond the scope of this paper.

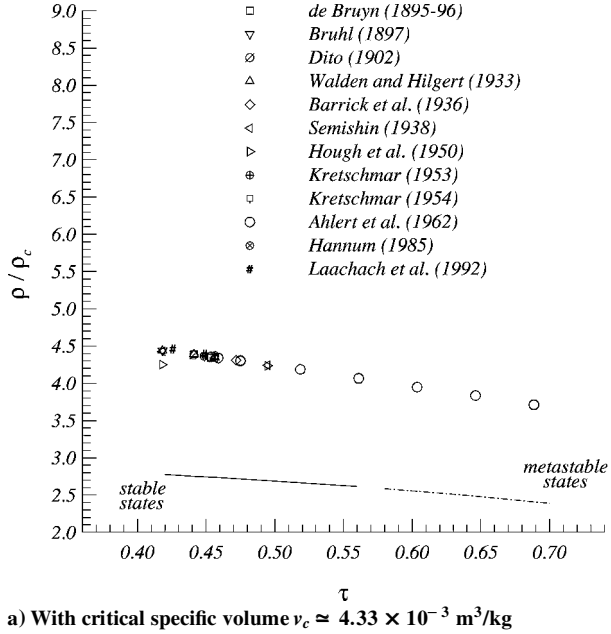

a) With critical specific volume $v_c \cong 4.33 \times 10^{-3}$ m^3/kg

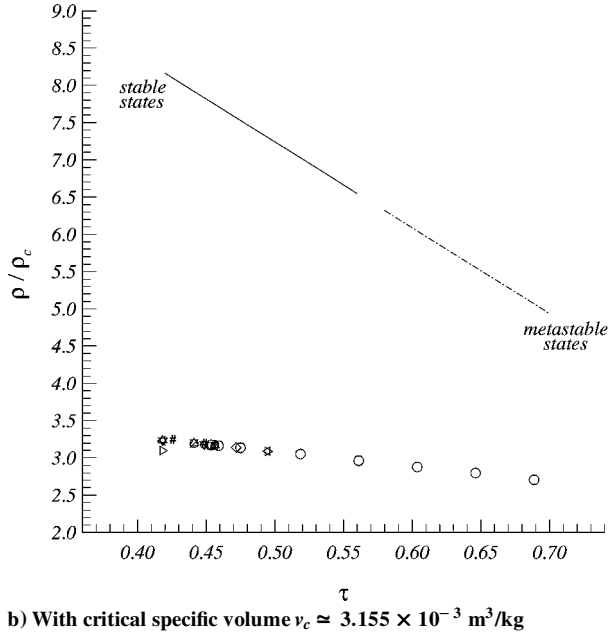

b) With critical specific volume $v_c \cong 3.155 \times 10^{-3}$ m^3/kg

Fig. 9 Density of liquid phase; experimental data and theoretical prediction of the present model ($n = 0.7$) at atmospheric pressure ($\pi \simeq 0.00689$).

C. Constant-Pressure Specific Heat of the Liquid Phase

In the Helmholtz-potential formulation, the constant-pressure specific heat can be obtained from the general formula

$$c_p = c_v + \frac{T v^2}{a_N^2}\left(\frac{\partial p}{\partial T}\right)_v^2 \tag{55}$$

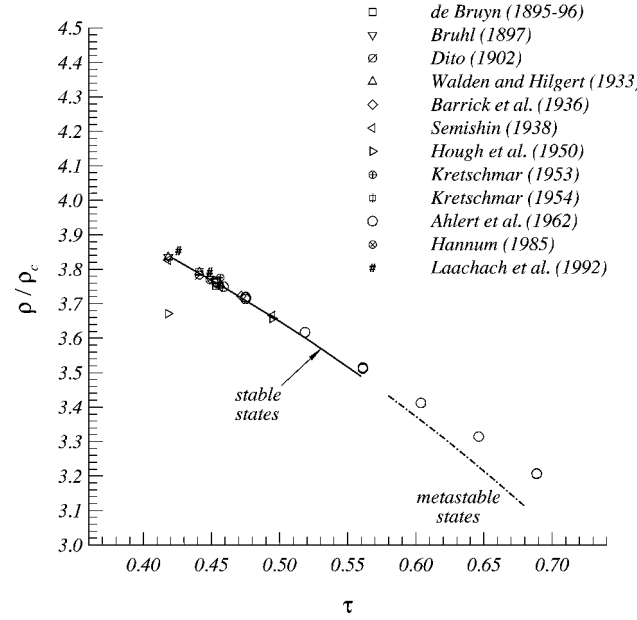

Fig. 10 Density of liquid phase; experimental data and theoretical prediction of the present model ($n = 0.7$) at atmospheric pressure ($\pi \cong 0.00689$) with $v_c = 3.740 \times 10^{-3}$ m^3/kg.

applicable to any thermodynamic system with two specific degrees of freedom. The thermodynamic parameters appearing on the right-hand side of Eq. (55) are easily determined. The constant-volume specific heat

$$c_v = \Phi(T) + \frac{n(n+1)C}{T^{n+1}(v+B)} \tag{56}$$

follows from Eq. (23) after substitution of Eq. (24). The squared isothermal speed of sound $a_N^2 = -v^2(\partial p/\partial v)_T$ and the derivative $(\partial p/\partial T)_v$ are obtained from straightforward derivation of the state equation [Eq. (6)] of the present model. Their expressions read, respectively,

$$a_N^2 = RT\left(\frac{v}{v-A}\right)^2\left[1 - \frac{2C(v-A)^2}{RT^{n+1}(v+B)^3}\right] \tag{57}$$

$$\left(\frac{\partial p}{\partial T}\right)_v = \frac{R}{v-A}\left[1 + \frac{nC(v-A)}{RT^{n+1}(v+B)^2}\right] \tag{58}$$

When Eqs. (57) and (58) are taken into account, Eq. (55) can be cast in nondimensional form as

$$\frac{c_p}{R} = \frac{c_v}{R} + \frac{\left[1 + \dfrac{27}{16}\dfrac{n}{\tau^{n+1}}\dfrac{\varphi}{(\varphi+1/2)^2}\right]^2}{\left[1 - \dfrac{27}{8}\dfrac{1}{\tau^{n+1}}\dfrac{\varphi^2}{(\varphi+1/2)^3}\right]} \tag{59}$$

in which

$$\frac{c_v}{R} = \frac{\Phi(T)}{R} + \frac{27}{16}\frac{n(n+1)}{\tau^{n+1}}\frac{1}{\varphi+1/2} \tag{60}$$

Analogous to the case of the liquid-phase density (see Sec. VI.B), to find out how the specific heats vary with temperature at a given pressure, the nondimensional state equation [Eqs. (15)] must be first solved for the unknown φ (left root); the latter value, then, must be substituted in Eqs. (59) and (60). Figure 11 shows the comparison between theoretical results relative to atmospheric pressure and experimental data[20,51,58] and reveals the existence of a noticeable discrepancy between the two classes of data. The experimental data appear to be in good agreement, and their characteristics have been discussed in Ref. 17. The present model with $n = 0.7$ performs poorly in this case. Unfortunately, there is no constant parameter left in the state equation [Eq. (6)] that could be tuned to reduce the divergence. The only way to bring the curve of the present model toward the experimental data would be to increase the exponent n; however, a change in the exponent compromises the reproduction of the liquid–vapor equilibrium curve (see Fig. 6). This situation certainly highlights a negative feature of the present model that calls for improvement.

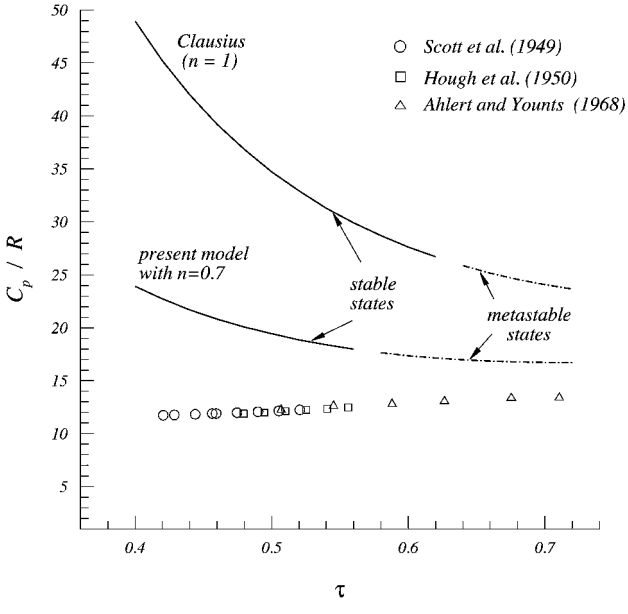

Fig. 11 Constant-pressure specific heat of the liquid phase; experimental data and theoretical predictions at atmospheric pressure ($\pi \simeq 0.00689$).

VII. Conclusions

The accurate prediction of N_2H_4 flows with phase changes presupposes the choice of a thermodynamic model of the compound that possesses basically two mandatory features: 1) the theoretically builtin capability to account for phase changes in the whole region of the (T, v) plane that is of interest for a given application (see Sec. II) and 2) the validated capability to reproduce experimentally determined thermodynamic properties of N_2H_4. With regard to these aspects, characteristics and limitations of old thermodynamic models[23–25] available in the literature have been discussed in Sec. IV. The model developed recently by Barragan et al.[26,27] and the one presented in this paper possess feature 1) for liquid–vapor phase transitions from 273.15 K ($\tau \simeq 0.42$) up to the critical point. With respect to the older models, they offer a better approximation to the experimental saturation-curve data. In this regard, however, note that the prediction capability of any model in the vicinity of the critical point inherits a degree of uncertainty from the experimental data available in that temperature neighborhood (solid squares in Fig. 6) because these are rather old and of uncertain origin.[17] Concerning feature 2 the present model secures the correct perfect-gas behavior at low density. Moreover, it produces a vaporization-enthalpy curve whose consistency and validity can be defended against the disagreement with data estimated by other authors[1,20,24,26,27,38,42,43] (see also Ref. 17 in this regard). With the critical specific volume tuned to $v_c = 3.740 \times 10^{-3}$ m^3/kg, it predicts satisfactorily the experimental data of the density of the liquid phase. Unfortunately, it does not perform well in reproducing the constant-pressure specific heat of the liquid phase. This drawback indicates the necessity to carry out additional refinement work about the model's state equation [Eq. (6)] to remove such a weak point. Nevertheless, the model has been implemented in a two-phase flow solver[59] and has proven to be well adapted for computational fluid dynamics analyses.

Acknowledgments

The authors wish to acknowledge the valuable advice and suggestions provided by L. Marraffa during several discussions related to the present work. Moreover, the authors are grateful to E. Schmidt and H. Nelson for their help in the procurement of Refs. 26 and 27.

References

[1] Schmidt, E., *Hydrazine and Its Derivatives*, Wiley, New York, 1984.

[2] Reijnen, B., "Droit Spatial International, les Règles du Jeu," *CNES Magazine*, No. 4, 1999, p. 24.

[3] Foucaud, R., d'Herbigny, F. X., Marraffa, L., Giordano, D., and Reynier, P., "Experimental Study of the Ariane 5 Attitude Control System (SCA) Passivation," AIAA Paper 2001-2763, June 2001.

[4] Tisza, L., *Generalized Thermodynamics*, MIT Press, Cambridge, MA, 1977.

[5] Callen, H., *Thermodynamics*, Wiley, New York, 1963.

[6] Callen, H., *Thermodynamics and an Introduction to Thermostatistics*, Wiley, New York, 1985.

[7] Napolitano, L., *Thermodynamique des Systèmes Composites en Équilibre ou Hors d'Équilibre*, Gauthier-Villars Éditeurs, Paris, 1971.

[8] Robertson, H., *Statistical Thermophysics*, Prentice–Hall, Englewood Cliffs, NJ, 1993.

[9] Poincaré, H., *Thermodynamique*, Éditions Jacques Gabay, Paris, 1995.

[10] Planck, M., *Treatise on Thermodynamics*, Dover, New York, 1990.

[11] Zemansky, M., and Dittman, R., *Heat and Thermodynamics*, McGraw–Hill, New York, 1981.

[12] Hirschfelder, J., Curtiss, C., and Bird, R., *Molecular Theory of Gases and Liquids*, Wiley, New York, 1964.

[13] Hill, T., *An Introduction to Statistical Thermodynamics*, Dover, New York, 1986.

[14] Hill, T., *Statistical Mechanics*, Dover, New York, 1987.

[15]Anderko, A., "Equation-of-State Methods for the Modelling of Phase Equilibria," *Fluid Phase Equilibria*, Vol. 61, 1990, pp. 145–225.

[16]Redlich, O., and Kwong, J., "On the Thermodynamics of Solutions," *Chemical Reviews,* Vol. 44, 1948, pp. 233–244.

[17]Giordano, D., "Survey of the Thermodynamic Properties of Hydrazine," *Journal of Chemical and Engineering Data,* Vol. 46, No. 3, 2001, pp. 486–505.

[18]Boltzmann, L., *Lectures on Gas Theory*, Dover, New York, 1995, pp. 210, 211.

[19]Wisniak, J., and Golden, M., "Predicting Saturation Curve of a Pure Substance Using Maxwell's Rule," *Journal of Chemical Education*, Vol. 75, No. 2, 1998, pp. 200–203.

[20]Scott, D., Oliver, G., Gross, M., Hubbard, W., and Huffman, H., "Hydrazine: Heat Capacity, Heats of Fusion and Vaporization, Vapor Pressure, Entropy and Thermodynamic Functions," *Journal of the American Chemical Society*, Vol. 71, 1949, pp. 2293–2297.

[21]Chase, M., "NIST–JANAF Thermochemical Tables," *Journal of Physical and Chemical Reference Data*, Monograph 9, pp. 1350, 1351.

[22]Gurvich, L., Veyts, I., and Alcock, C., *Thermodynamic Properties of Individual Substances*, Vol. 1, Pt. 1, Hemisphere, New York, 1989, p. 225.

[23]Haws, J., and Harden, D., "Thermodynamic Properties of Hydrazine," *Journal of Spacecraft and Rockets*, Vol. 2, No. 6, 1965, pp. 972–974.

[24]Das, T., and Kuloor, R., "Thermodynamic Properties of Hydrazine," *Journal of the Indian Institute of Science,* Vol. 50, No. 1, 1968, pp. 13–25.

[25]Tsykalo, A., Savenkov, V., Selevanyuk, V., and Yakushev, A., "Thermodynamic Properties of Hydrazine," *Journal of Applied Chemistry (USSR)*, Vol. 47, 1974, pp. 437–439.

[26]Barragan, M., Woods, S., and Wilson, D., "An Equation of State for Hydrazine and Monomethylhydrazine, Its Validation and Use for Calculation of Thermodynamic Properties," Chemical Propulsion Information Agency, CPIA Publ. 674, Vol. 1, Laurel, MD, 1998, pp. 191–201.

[27]Barragan, M., Woods, S., Julien, H., Wilson, D., and Saulsberry, R., "A Multiphase Equation of State for Hydrazine and Monomethylhydrazine," AIAA Paper 99-2418, June 1999.

[28]Martin, J., and Hou, Y., "Development of an Equation of State for Gases," *American Institute of Chemical Engineers Journal*, Vol. 1, No. 2, 1955, pp. 142–151.

[29]Martin, J., Kapoor, R., and De Nevers, N., "An Improved Equation of State for Gases," *American Institute of Chemical Engineers Journal*, Vol. 5, No. 2, 1959, pp. 159, 160.

[30]Yaws, C., *Physical Properties: A Guide to the Physical, Thermodynamic and Transport Property Data of Industrially Important Compounds*, McGraw–Hill, New York, 1977.

[31]Gibbs, J., "On the Equilibrium of Heterogeneous Substances," *Transactions of the Connecticut Academy*, Vol. 3, 1876, pp. 108–248 and Vol. 3, 1878, pp. 343–524.

[32]Gibbs, J., *The Scientific Papers of J. Willard Gibbs: Thermodynamics*, Ox Bow Press, Woodbridge, CT, 1993.

[33]Fermi, E., *Thermodynamics*, Dover, New York, 1956.

[34]Denbigh, K., *The Principles of Chemical Equilibrium*, Cambridge Univ. Press, Cambridge, England, U.K., 1993.

[35]Lobry de Bruyn, C., "Ueber das Freie Hydrazin," *Berichte der Deutschen Chemischen Gesellschaft*, Vol. 28, 1895, pp. 3085, 3086.

[36]Lobry de Bruyn, C., "L'Hydrazine Libre I.," *Recueil des Travaux Chimiques des Pays Bays*, Vol. 15, 1896, pp. 174–184.

[37]West, C., and Hull, C., (eds.), *International Critical Tables of Numerical Data, Physics, Chemistry and Technology*, Vol. 3, McGraw–Hill, New York, 1933, pp. 228, 229.

[38]Hieber, W., and Woerner, A., "Thermochemische Messungen an Komplexbildenden Aminen und Alkoholen," *Zeitschrift für Elektrochemie*, Vol. 40, No. 5, 1934, pp. 252–256.

[39]Burtle, J., "Vapour Pressure-Composition Measurements on Aqueous Hydrazine Solutions," *Industrial Engineering Chemistry*, Vol. 44, No. 7, 1952, pp. 1675, 1676.

[40]Chang, E., and Gokcen, N., "Thermodynamic Properties of Hydrazine, Unsymmetrical Dimethylhydrazine, and Their Mixtures," The Aerospace Corp., Rept. ATN-64(9228)-2, El Segundo, CA, 1964.

[41]Hannum, J., "Hazards of Chemical Rockets and Propellants. Volume 3: Liquid Propellants Manual," Chemical Propulsion Information Agency, CPIA Rept. AD-A158115, Laurel, MD, 1985.

[42]Fresenius, W., and Karweil, J., "Die Normalschwingungen und die Konfiguration des Hydrazins. II. Das Ultrarotspektrum des Hydrazins," *Zeitschrift für Physikalische Chemie*, Vol. 44, No. 1, 1939, pp. 1–13.

[43]Giguere, P., "Spectroscopic Evidence of Hydrogen Bonds in Hydrogen Peroxide and Hydrazine," *Transactions of the Royal Society of Canada*, Vol. 35, May 1941, pp. 1–8.

[44]Reid, R., Prausnitz, J., and Poling, B., *The Properties of Gases and Liquids*, McGraw–Hill, New York, 1987, p. 219.

[45]Lobry de Bruyn, C., "De Bereidingswijze en de Eigenschappen van het Hydrazine," Berichten der Koninklijke Akademie der Wetenschappen (Amsterdam), Vol. 4, 1895, pp. 73, 74.

[46]Brühl, J., "Spectrochemistry of Nitrogen—V," *Zeitschrift für Physikalische Chemie*, Vol. 22, 1897, pp. 373–409 (in German).

[47]Dito, J., "The Densities of Mixtures of Hydrazine and Water," Berichten der Koninklijke Akademie der Wetenschappen (Amsterdam), Vol. 4, 1902, pp. 756–758.

[48]Walden, P., and Hilgert, H., "Anhydrous Hydrazine as an Ionization Medium for Electrolytes and Nonelectrolytes," *Zeitschrift für Physikalische Chemie*, Vol. 165A, 1933, pp. 241–271 (in German).

[49]Barrick, L., Drake, G., and Lochte, H., "The Parachor and Molecular Refraction of Hydrazine and Some Aliphatic Derivatives," *Journal of the American Chemical Society*, Vol. 58, 1936, pp. 160–162.

[50]Semishin, V., "Internal Friction and Fusibility of the System Hydrazine-Water," *Journal of General Chemistry (USSR)*, Vol. 8, 1938, pp. 654–661 (English summary).

[51]Hough, E., Mason, D., and Sage, B., "Heat Capacity of the Hydrazine-Water System," *Journal of the American Chemical Society*, Vol. 72, 1950, pp. 5774, 5775.

[52]Kretschmar, G., "The Velocity of Sound in Some Rocket Propellant Liquids," *American Rocket Society Journal*, Vol. 23, 1953, pp. 82–84.

[53]Kretschmar, G., "The Isothermal Compressibilities of Some Rocket Propellant Liquids, and the Ratio of the Two Specific Heats," *Jet Propulsion*, Vol. 24, May 1954, pp. 175–186.

[54]Ahlert, R., Bauerle, G., and Lecce, J., "Density and Viscosity of Anhydrous Hydrazine at Elevated Temperatures," *Journal of Chemical and Engineering Data*, Vol. 7, No. 1, 1962, pp. 158–160.

[55]Laachach, A., Ferriol, M., Cohen-Adad, M.-T., Huck, J., Jorat, L., Noyel, G., Getzen, F., and Bureau, J., "Densities, Molar Volumes and Viscosities in the Systems Water–Hydrazine, Water–Methylhydrazine and Water–1,1–Dimethylhydrazine," *Fluid Phase Equilibria*, Vol. 71, 1992, pp. 301–312.

[56]Audrieth, L., and Ogg, B., *The Chemistry of Hydrazine*, Wiley, New York, 1951.

[57]Bellajrou, R., "Équilibres Liquid-Vapeur. Application au Système Ternaire NH_3-CH_3NH_2-H_2O. Tensions de Vapeur et Cinétique de Décomposition de N_2H_4, $(CH_3)_2NNH_2$ et UH25," Ph.D. Dissertation (30-92), Université Claude Bernard, Lyon I, France, 1992.

[58]Ahlert, R., and Younts, C., "Heat Capacities of 90% Hydrogen Peroxide and Commercial Anhydrous Hydrazine," *Journal of Chemical and Engineering Data*, Vol. 13, No. 3, 1968, pp. 402–405.

[59]Reynier, P., Wesseling, P., Marraffa, L., and Giordano, D., "Computation of Liquid Hydrazine Depressurization with a Mach Uniform Staggered Grid," *Journal of Flow, Turbulence and Combustion*, Vol. 66, 2001, pp. 113–132.